EXPERIMENTAL ANALYSIS OF A COAXIAL SOLID-PROPELLANT MPD THRUSTER WITH SEGMENTED ANODES [1]

G. Paccani [2]

Universita' di Roma "La Sapienza", Rome, Italy

Abstract

A quasisteady solid-propellant MPD propulsion system utilizing coaxial breech-fed and side-fed thrusters with segmented and entire - cylindrical and diverging - anodes was investigated. Current flowing in each anode segment, as well as propellant consumption and jet velocity were measured. The same was done on similar entire-anode thrusters, the thrust of which was also measured.

The anodic current distribution reaches its peak in the central segments, particularly in the second one. In the final segments of the longest anodes it is quite negligible. The current describes a time profile which varies in the different segments.

In all side-fed thrusters, current, propellant consumption and jet velocity almost coincide in all configurations, with the only exception of mass consumption, which is lower in entire-anode thrusters than in segmented-anode thrusters.

The thrust is in any case linearly increasing with squared current; it is higher in diverging-anode thrusters than in cylindrical ones.

On the whole, the results confirm the hypothesis of a "self-regulating" behaviour on the part of solid-propellant thrusters - in particular side-fed thrusters - which implies the same functioning, characterized by the same $K=I^2/\dot{m}$, in all regimes.

Better performances are expected by adopting smaller propellant surface areas exposed to the discharge and larger r_a/r_c radius ratios.

Nomenclature

A = pendulum oscillation maximum amplitude
A_p = propellant surface area exposed to the discharge
C = PFN capacity
E_0 = initial energy stored in the PFN
E_p = (measured) thruster energy per shot
f = frequency
F = thrust
I = current
I_b = impulse bit
K = $I^2/\dot{m}$
M = mass
m = mass per shot
$\dot{m}$ = mass flow rate
N = number of samples
P = power
PFN = pulse-forming network
r_a = thruster anode radius
r_c = thruster cathode radius
V = voltage
V_0 = initial PFN charge voltage
w = (measured) jet velocity
μ_0 = magnetic permeability
ρ = r_a/r_c
σ_x = standard error on x
σ_{yx} = $[\Sigma(y-y_{est})^2/N]^{1/2}$ standard error of estimate of y on x
τ = thruster discharge duration
ω = pendulum pulsation

Subscripts

acc = accelerated
cyl = cylindrical
div = diverging
e = effective, equivalent
EA = entire anode
est = estimate
exp = experimental
l = loss
p = propellant, propulsion
SA = segmented anode
sp = specific
th = theoretical
% = per cent

1 - Introduction

The present paper describes a progressive experimental analysis of the functioning of a high power (≈1÷3 MW) solid-propellant (Teflon) quasisteady coaxial MPD thruster. Previous works [1] have been carried out, based on the experimental study of the working parameters with varying energy per shot ($E_0=1/2\ CV_0^2$). The results of those works induce to consider the global functioning of a solid-propellant propulsion system described by relations that, with increasing power, may be reduced to the following ones:

$$I^2 = K_1 E_0 , \qquad (1)$$

[1] This research is supported by ASI (Agenzia Spaziale Italiana) and MURST (Ministero dell'Universita' e della Ricerca Scientifica e Tecnologica).

[2] Senior Research Engineer, Dipartimento di Meccanica e Aeronautica, Member AIAA.

$$\dot{m} = K_3 E_0 ; \qquad (2)$$

K_1 K_3 being constant; hence,

$$K = \frac{I^2}{\dot{m}} = constant. \qquad (3)$$

From a physical point of view, ablation depends on the energy electrically dissipated in the vicinity of the propellant surface [2]; it might depend on the spatial distribution of current density. Thus, it seems useful to investigate the possible connection between this distribution and the thruster functioning. An experimental investigation was carried out on long-anode (arc chamber 72÷102 mm long) short-cathode thrusters. With that configuration, the cathodic current is concentrated on a very limited area; thus the determination of the anodic current distribution alone may provide rough but significant information on the spatial distribution of current itself.

The anodic current distribution was investigated utilizing segmented-anode (SA) thrusters. These anodes (Figs 1, 2) consist of a series of segments - each being electrically insulated from the others - all powered by the same PFN. From an electrical point of view, the thruster can be sketched as impedances connected in parallel. This arrangement enables to measure the current flowing to each segment.

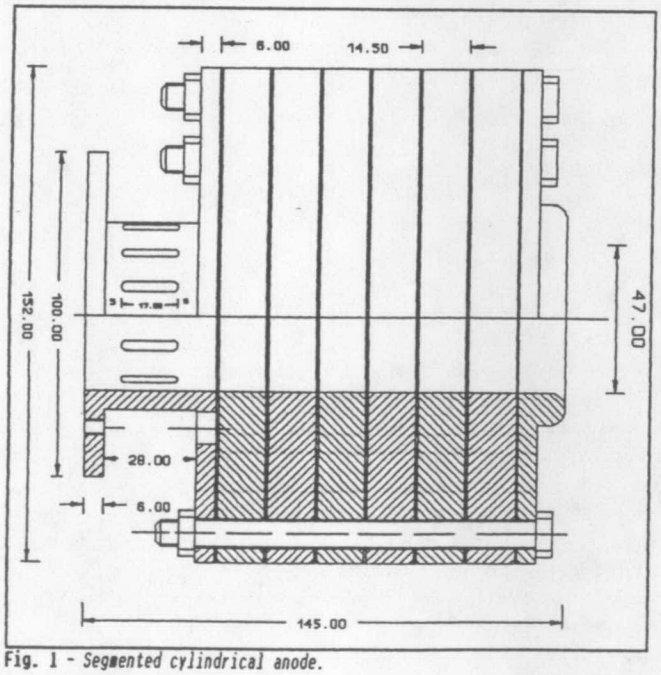

Fig. 1 - *Segmented cylindrical anode.*

This work is based on the contemporary experimental measurements of the thruster parameters - functioning and performance - and of current density distribution along the anode.

The functioning of these segmented-anode thrusters was then compared with that of geometrically similar thrusters utilizing an entire (non segmented) anode (EA).

Thrusters with cylindrical and diverging anodes of different length were investigated in the whole working power range. In every segmented-anode thruster the current flowing through each segment, as well as propellant consumption and jet velocity have been measured. The same was done on similar entire-anode thrusters, the thrust of which was also measured.

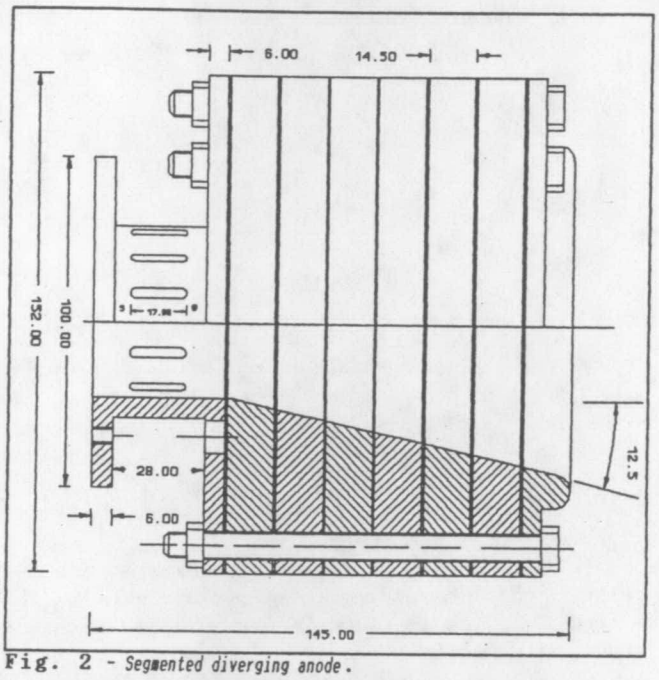

Fig. 2 - *Segmented diverging anode.*

2 Experimental Apparatus

2.1 Vacuum facilities

Two vacuum facilities were used: a former, with a Plexiglas vacuum tank 1 m in length and inner diameter of 0.50 m, for the segmented-anode thrusters measurements and a latter, with a PVC vacuum tank 1,30 m in length and inner diameter of 0.675 m, for the investigation of a "modular" entire-anode thruster. A 25-cm oil diffusion pump and two 60 m^3/h mechanical backing pumps operated on each tank. In all experiments the tank pressure was maintained to less than 10^{-4} mbar between each firing.

2.2 Propulsion systems

The thrusters consist of a structure of independently interchanging modules. Both "*breech-fed*" (Fig. 3) and "*side-fed*" (Fig. 4) configurations are feasible. They are based on an insulating-material (PVC) "*base module*" on which the following elements can be assembled:

- the anode-nozzle on which the side-feeding device can be assembled;
- an element of insulating and arc-resistant material

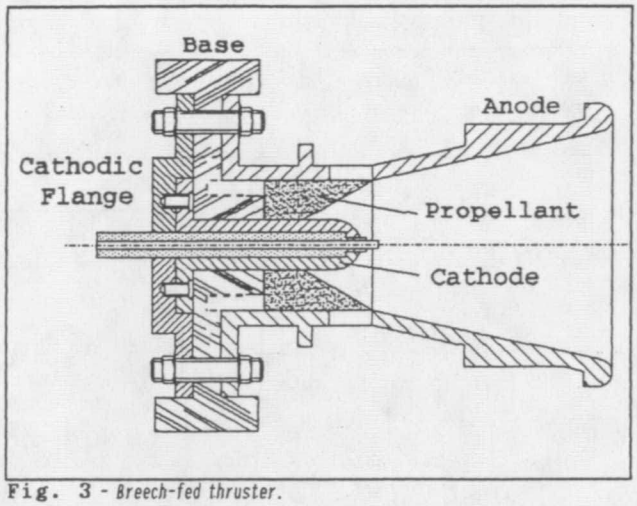

Fig. 3 - *Breech-fed thruster.*

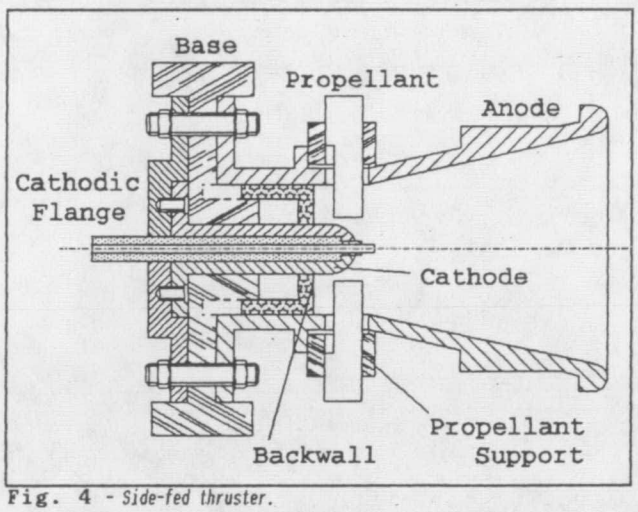

Fig. 4 - *Side-fed thruster.*

(Stumatite) forming the backwall of the thrust chamber (in side-fed thrusters only), the position of which can be regulated;
- the cathodic flange on which the cathode is assembled;
- breech-fed propellant.

The entire anodes have an initial cylindrical part, with an inner length of 58 mm and an internal diameter of 47 mm; the downstream part is cylindrical or diverging with a divergence angle of 12.5^0. The cylindrical cathodes have an hemispherical tip; in this study only the last hemispherical part of the cathode surface protrudes from the breech.

The segmented anodes (Figs. 1, 2) are built assembling 14.5-mm-long components on an initial element meant for propellant feeding; the elements are electrically divided one from the other with insulating and arc-resistant 5-mm-thick discs; the portion of the arc chamber in the initial element is 27 mm long.

The propellant consists of six 3-mm Teflon bars radially inserted in the discharge chamber through suitable slots. Their axial dimension is 11 mm. The total surface area exposed to the discharge (A_p) equals 25 cm^2.

All thrusters were powered by the same capacitor bank (Pulse-Forming Network, PFN) of 30 elements (each formed by an electrolytic capacitor plus inductor) with a total capacity of about 60 mF and a maximum charge voltage of 450 V. The "equivalent" discharge duration (τ) is of about 1 ms.

The thruster firing is triggered off by a device supplying a voltage pulse to a cylindrical tungsten electrode of 2 mm in diameter; this electrode axially protrudes from the cathode tip (at ground potential). The pulse voltage maximum value is programmable in the range 0÷20 kV, while pulse duration is very short (a few microseconds) not to bias measurements.

2.3 Diagnostics

All measurements are computerized. All signals provided by the instruments are sent to analog/digital oscilloscopes with high sample rate [Philips PM 3315 (f= 100 MHz), Philips PM 3394 (f=200 MHz)] and then transferred to a personal computer.

2.3.1 Currents - The actual currents were measured with multiprobe Rogowsky devices with operational amplifiers (Fig. 5).

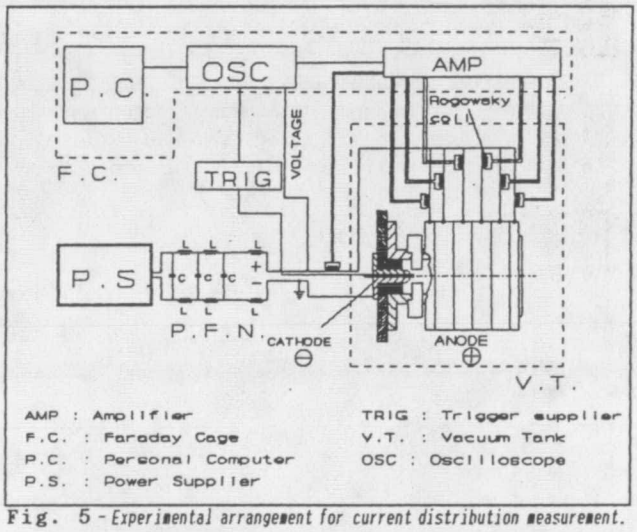

Fig. 5 - *Experimental arrangement for current distribution measurement.*

2.3.2 Mass consumption - Mass consumption was measured with a 1-mg precision electronic balance.

2.3.3 Jet Velocity - The plume velocity was measured through the time-of-flight method. The time-of-flight was calculated through a computerized cross-correlation of the saturation currents of two double Langmuir probes acting as targets [4].

The probes (Fig. 6) are such that the electrodes define a plane with the necessary precision. The electrodes are made of tungsten wires partially included in quartz tubes assembled on a Plexiglas frame. Their extremes are rolled up on Nylon screws

transmitting the necessary tension to the wires. A Teflon tape insulates the wire extremes from the plume. The procedure was optimized according to the instrumentation adopted: assuming that plasma oscillation was frozen in the flux, the theoretical relative uncertainty was reduced to about 1%.

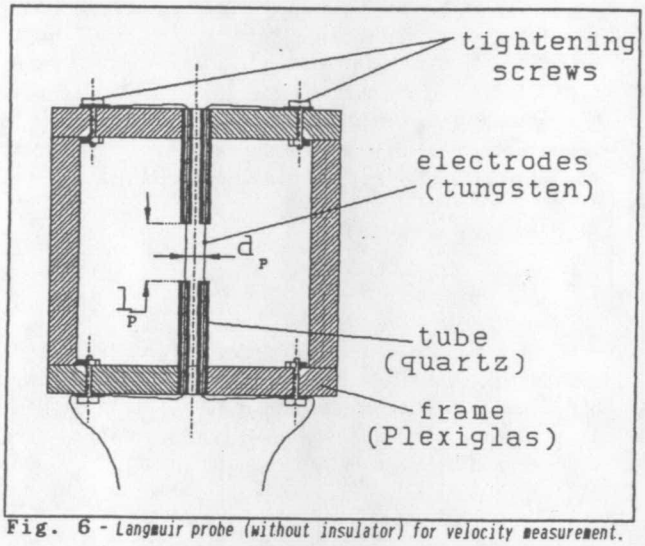

Fig. 6 - *Langmuir probe (without insulator) for velocity measurement.*

2.3.4 Impulse bit - The impulse bit (Fig. 7) was measured with a parallelogram-pendulum thrust stand on which the thrusters were fixed. The oscillating system motion produced by a shot was measured with an inductive contactless transducer [HBM Tr 102]. Electrical power was supplied by mercury-filled pots to enable free oscillation of the pendulum.

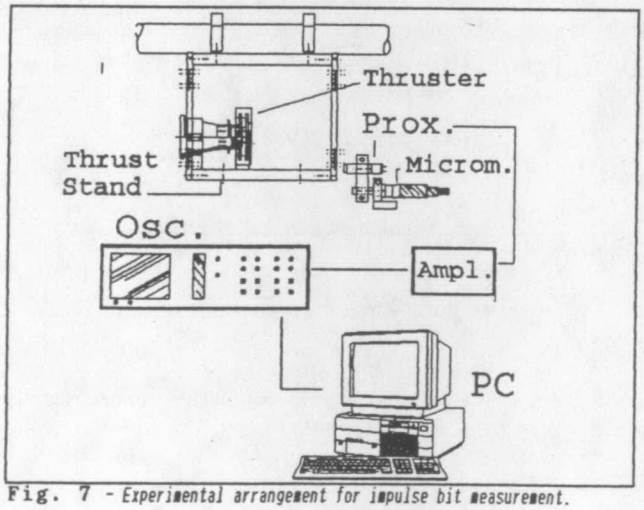

Fig. 7 - *Experimental arrangement for impulse bit measurement.*

The impulse bit is obtained by the equation [4]:

$$I_b = MA\omega \ , \qquad (4)$$

where M is the mass of the equivalent simple pendulum, A is the maximum oscillation amplitude and ω is the pendulum pulsation. M is obtained by an experimental dynamic calibration of the system; A is computed through the exponential fit of 6÷8 periods of the displacement curve (Fig. 8); ω is calculated through the Fast Fourier Transform operated on 120÷160 periods of the displacement curve.

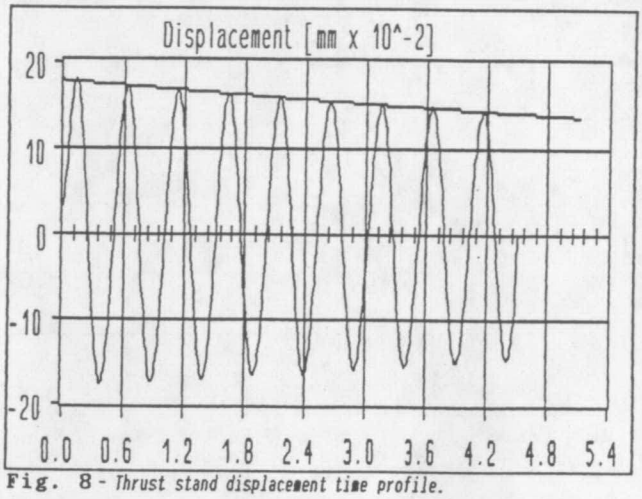

Fig. 8 - *Thrust stand displacement time profile.*

3 Experimental Analysis

3.1 Parameters

The impedance connected with the PFN depends on the different thruster and transmission line configurations adopted as well as on the different power regimes. Generally speaking, the discharge has its own time profile in each case. Therefore, to carry out a comparative system analysis in different cases, either integral parameters relative to the whole shot are adopted, or the time-dependent actual thruster functioning is replaced by an "*equivalent*" fictitious quasisteady functioning described by conventional parameters ["*equivalent*" (or "*effective*") parameters]; these last parameters are obtained assuming as conventional arc duration (τ) the lapse of time the arc needs to absorb a given quantity of the total shot energy

$$E_p = \int_0^{\bar{\tau}} V I \, dt \, ; \qquad (5)$$

i. e.:

$$\int_0^{\tau} V I \, dt = \alpha E_p \, ; \qquad (6)$$

hence

$$I^2 = \frac{\Psi}{\tau}, \qquad (7)$$

$$Z = \frac{E_p}{\Psi}, \qquad (8)$$

being

$$\Psi = \int_0^{\infty} I^2(t)\, dt. \qquad (9)$$

In the present study ε=0.98.

3.2 Experiments

Experiments concern the following side-fed thrusters:

- thrusters with cylindrical and diverging (benchmark) entire anodes with a 86-mm-long arc chamber;
- thrusters with cylindrical and diverging segmented anodes respectively utilizing 4 and 6 segments: the 6-segment anodes form an arc chamber identical to that of the entire anodes, while the former are 30 mm shorter.

Moreover, a 6-segment anode thruster was tested supplying power to the first two segments only.

Each configuration was tested according to seven values of the PFN initial energy, E_0. The values were in the 1÷3 kJ range every 333 J and were imposed by fixing the PFN initial charging potential, V_0. Assuming that the τ discharge duration was constant, all that equals considering seven power regimes in the ≈1÷3 MW range.

For each configuration and working regime the following quantities were measured:

- time-profile of the actual total current and of the actual current flowing in each segment as well as the conventional τ, Ψ, and I parameters; for each of them the mean of a sample of 20 is assumed as best value being σ_I<1% for quantities relative to the whole thruster and σ_I<2% for those relative to each segment;
- propellant consumption per shot; it is obtained weighing the propellant before and after a number of shots ensuring a consumption higher than 50 mg;
- jet velocity (w); the mean of a sample of 30 values is assumed as best value being σ_w<2%;
- impulse bit in entire-anode thrusters; the mean of a sample of 5 values is assumed as best value being σ_I<1%.

Thrust measurement is impossible on segmented-anode thrusters as the large number of electrical connections does not allow the oscillation of the thrust stand oscillating system.

A preliminary phase of investigation aiming at verifying the working and set up of the experimental method was carried out on a breech-fed thruster powered by two different PFNs (a quasipulsed one and a quasisteady one). Segmented anodes with 25-mm-long segments were adopted.

4 Results

4.1 Current distribution in segmented anodes

The anode-forming segments are considered in increasing order according to the flux direction.

As already pointed out, the first segment, which contains the feeding device, was longer than the others; thus elaborating the data of this segment, the quantities scaled to the length of the other segments are considered. The quantities in each segment are then examined starting from the first segment.

4.1.1 Six-segment anode thrusters. The behaviour of the six-segment anode thrusters (Figs. 9÷12) is very similar in both configurations (diverging and cylindrical anode).

The Ψ parameter (Figs. 9, 11) rapidly increases, reaching its maximum in the second segment, and then decreases till it attains, in the fourth segment, values comparable to those of the first. In diverging anodes, it assumes almost negligible values starting from the fourth segment. In some cases, with higher power, the last segment shows slightly higher values as against the last but one. That is probably due to the edge effect. Quite the reverse, impedance (Figs. 10, 12) reaches the minimum in the second segment and then rises, attaining very high values in the last segments.

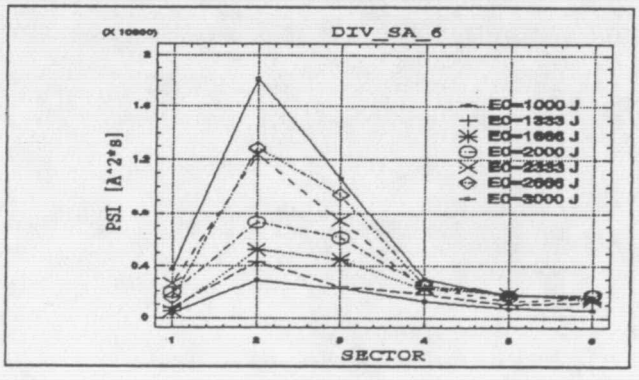

Fig. 9 - *Six-segment diverging-anode thruster; Ψ vs. segment.*

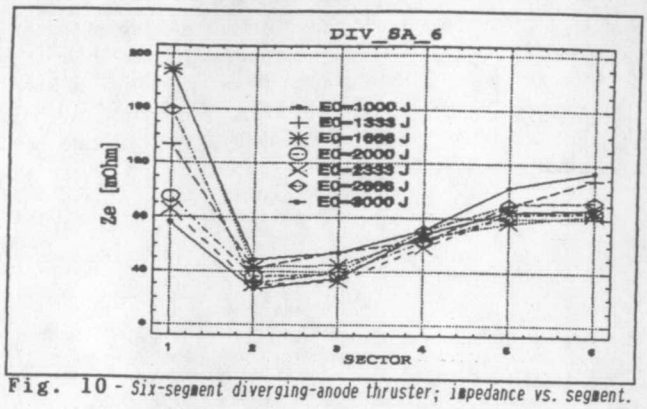

Fig. 10 - *Six-segment diverging-anode thruster; impedance vs. segment.*

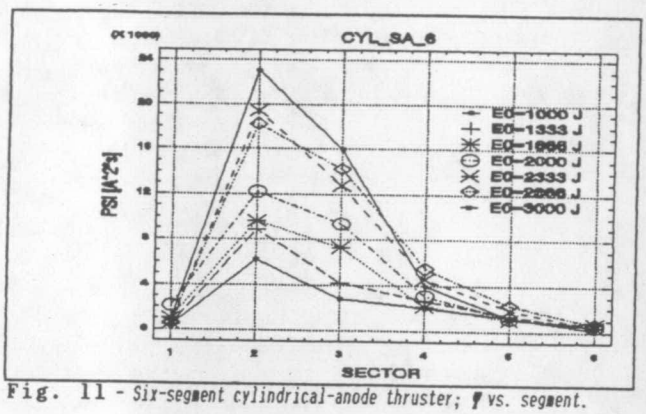

Fig. 11 - *Six-segment cylindrical-anode thruster; ψ vs. segment.*

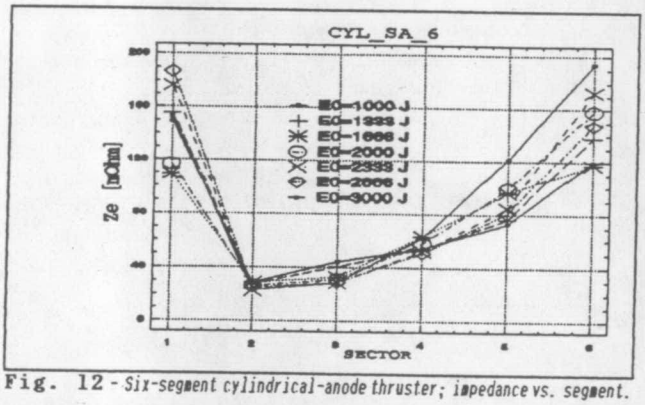

Fig. 12 - *Six-segment cylindrical-anode thruster; impedance vs. segment.*

4.1.2 Four-segment anode thrusters. In four-segment anode thrusters (Figs. 13÷16), the behaviour changes according to the anode (cylindrical or diverging).

In diverging anodes (Figs. 13, 14), in turn, two different behaviours emerge:

- for higher power, ψ (Fig. 13) behaves as it does in six-segment anode thrusters, though the trend is less marked;
- for lower power, ψ shows very poor values in the first segment, then following a monotone trend slightly increasing with the abscissa.

The different reactions to power variation are made even more evident by the impedance behaviour (Fig. 14).

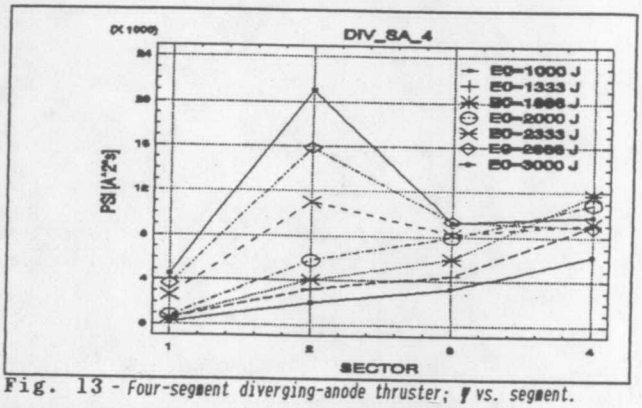

Fig. 13 - *Four-segment diverging-anode thruster; ψ vs. segment.*

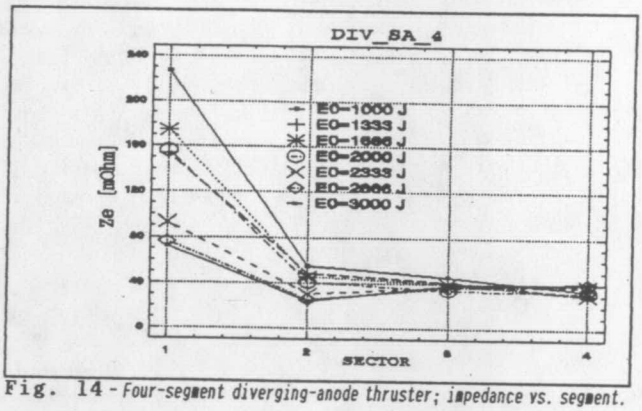

Fig. 14 - *Four-segment diverging-anode thruster; impedance vs. segment.*

In cylindrical anodes (Figs. 15, 16) ψ (Fig. 15) is higher in the second segment as against the first one and tends to remain almost constant in the three following segments. On the contrary, impedance (Fig. 16) is higher in the first segment and tends to remain almost constant in the three following segments.

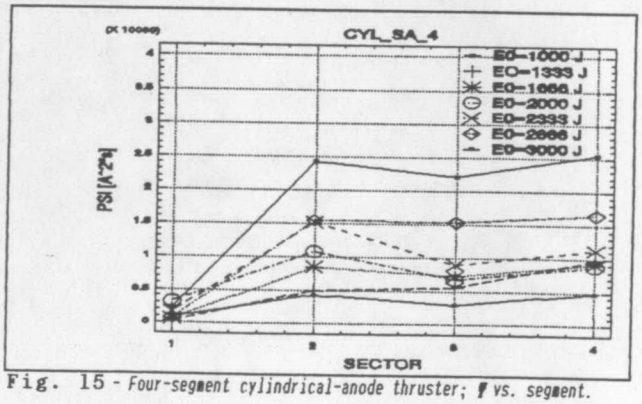

Fig. 15 - *Four-segment cylindrical-anode thruster; ψ vs. segment.*

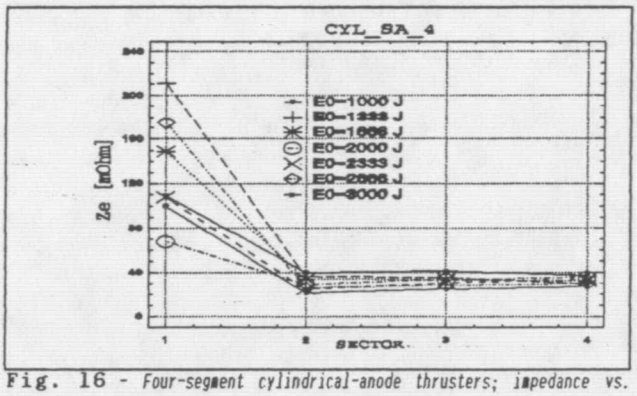

Fig. 16 - *Four-segment cylindrical-anode thrusters; impedance vs. segment.*

4.1.3 Current time profile - In each case, current shows a time profile which is different in each segment; in particular, the maximum is attained in subsequent moments during the whole discharge phase, starting from the last segment and following a backward path up to the first (Fig. 17).

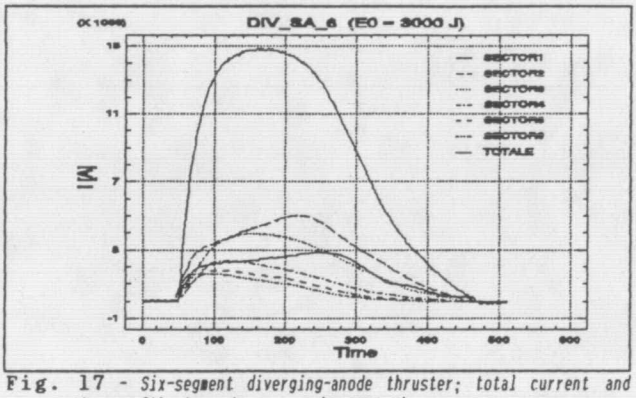

Fig. 17 - *Six-segment diverging-anode thruster; total current and current time profile in each segment (E_0=3000 J).*

4.2 Total Parameters

The parameters concerning the whole thruster as function of the PFN initial energy, E_0 are now considered.

In all cases - as expected [1] - Ψ (Fig. 18) and the propellant consumption, m (Fig. 19), are linearly increasing with E_0 with good approximation ($\sigma_{\Psi E} < 4*10^3$ A^{2}s, $\sigma_{mE} < 0.1$ mg).

In SA and EA thrusters respectively, those parameters show, in each regime, the same values for all geometries. Generally speaking, the parameter $K=I^2/\dot{m}=\Psi/m$ has constant values for each anodic solution. While Ψ takes up the same values in all thrusters, m shows slightly lower values in EA thrusters; hence

$$K_{EA} > K_{SA} \qquad (10)$$

being on average, considering all the different geometries, K_{EA}= 66÷67 KA^2*s/g and K_{SA}= 57÷61 KA^2*s/g.

Furthermore, the quantities relative to EA cylindrical-anode thrusters show a more irregular trend than those relative to diverging-anode thrusters.

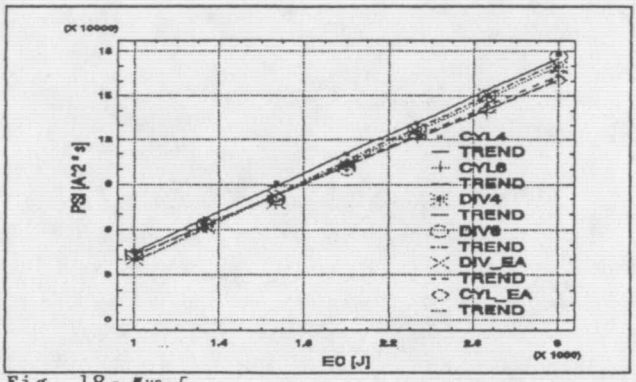

Fig. 18 - Ψ vs. E_0

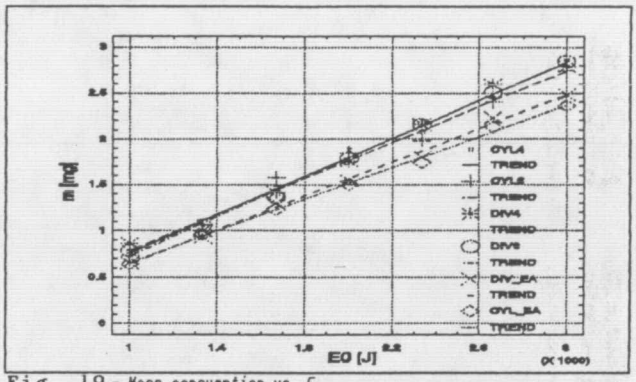

Fig. 19 - *Mass consumption vs. E_0*

The preliminary investigation on breech-fed SA thrusters showed trends similar to the previous ones but with some differences between cases.

As expected [1], impedance (Fig. 20) follows a decreasing trend and asymptotically tends towards a limit value.

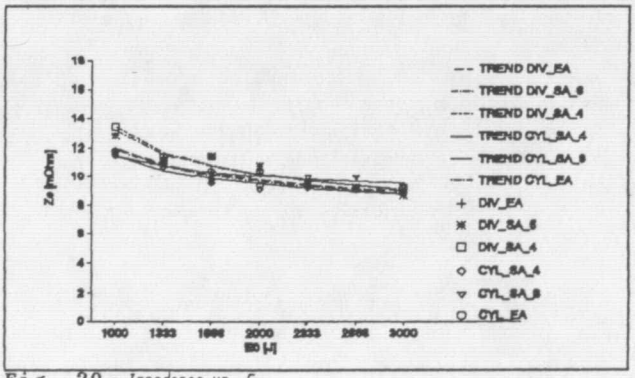

Fig. 20 - *Impedance vs. E_0*

4.3 Thrust

Impulse bit (Fig. 21) is linearly ($[\sigma_{FE}]_{div}$<0.3 N*ms, $[\sigma_{FE}]_{cyl}$<0.6 N*ms) increasing with E_0 and in cylindrical-anode thrusters it is on average about 12% lower.

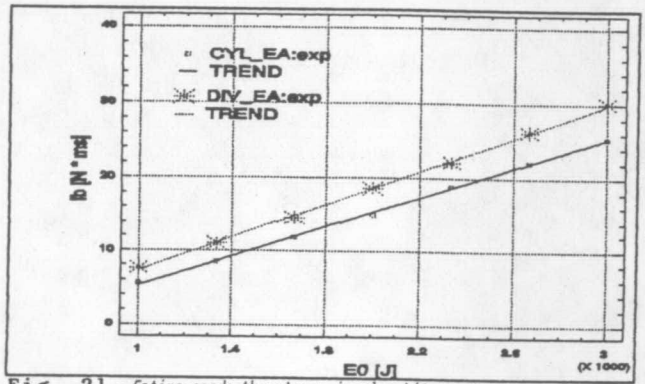

Fig. 21 - *Entire-anode thrusters; impulse bit vs. E_0*

The $f_{sp}=F/P_{PFN}=I_b/E_0$ ratio follows an increasing trend and asymptotically tends towards a limit value (fig. 22).

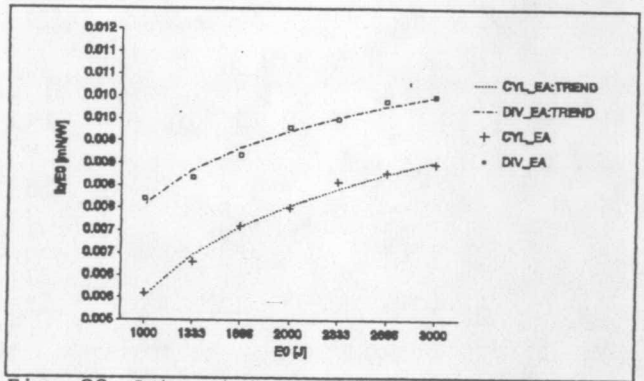

Fig. 22 - *Entire-anode thrusters; I_b/E_0 vs. E_0*

4.4 Jet Velocity

Jet velocity provided about the same figures in all thrusters; in each and every case, those values showed an irregular trend with varying E_0. For EA thrusters these values are located in the range $18.0*10^3$÷$18.9*10^3$ m/s (mean value equalling $18.5*10^3$ m/s). Considering the uncertainty of measurements due to the hypothesis of frozen oscillation in the flux, jet velocity is assumed constant in each thruster.

5 Concluding Remarks

The foregoing results give rise to some considerations.

Longer SA thrusters provide low currents and high impedances in the final anodic segments. On the other hand, longer diverging anodes produce no gasdynamic contribution leading to a detectable rise in jet velocity; all of which suggests that shorter anodes are more suitable.

All measured total parameters show the same values in side-fed SA thrusters; unlike what happens in breech-fed thrusters, they have the same behaviour with all anodic geometry. For what concerns the ablation process, the propellant position within the discharge makes side-fed thrusters less sensitive to anode geometry variations or to current distribution in general.

Indeed, functioning differences, involving mass consumption, emerge between SA and EA thrusters. That is mainly due to the different impedances current transmission line offers to PFN. That affects the current time-profile. Indeed, deviating from the optimum matching condition ($Z_{load}=Z_{PFN}$), it causes a remarkable distortion in the current profile as against the quasisteady one.

As already pointed out, Ψ (Fig. 18) and the impulse bit (Fig. 21) are, in all cases, linearly increasing with E_0; hence (Figs. 23, 24)

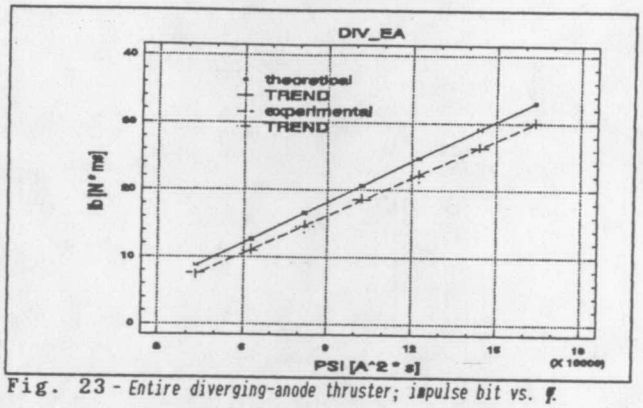

Fig. 23 - *Entire diverging-anode thruster; impulse bit vs. Ψ.*

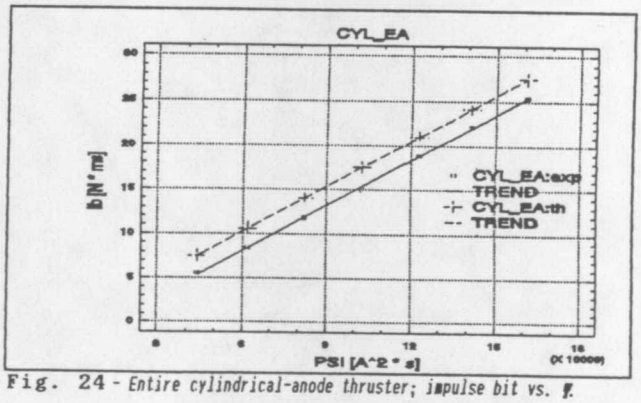

Fig. 24 - *Entire cylindrical-anode thruster; impulse bit vs. Ψ.*

$$I_b = a + b_{exp}\,\Psi \qquad (11)$$

being $|a_{cyl}|>|a_{div}|$, with $|a_{div}|$ almost negligible. Anyway, the relative value of $|a|$ decreases with increasing Ψ and thus E_0. In a first approximation this constant is neglected and mean experimental values of b_{exp} are considered; $[b_{exp}]_{div}= 1{,}79*10^{-7}$ H/m and $[b_{exp}]_{cyl}= 1{,}46*10^{-7}$ H/m are respectively obtained. The result is in good agreement with the theoretical well known equation [5]

$$F = bI^2 \qquad (12)$$

being

$$b = \frac{\mu_0}{4\pi}\left(\ln\frac{r_a}{r_c} + \frac{3}{4}\right) \qquad (13)$$

where r_a and r_c are respectively the anode and cathode radius; in which case, relation (13) respectively provides $[b]_{div} = 2.02*10^{-7}$ H/m and $[b]_{cyl} = 1{,}71*10^{-7}$ H/m, assuming as r_a its average value in the case of diverging anodes. Therefore

$$\beta_{div} = \left[\frac{b_{exp}}{b}\right]_{div} = 0.90\,, \qquad (14)$$

$$\beta_{cyl} = \left[\frac{b_{exp}}{b}\right]_{cyl} = 0.85\,.$$

The effective velocity

$$w_e = \frac{\sum_p \dot{m}_p w_p}{\sum_p \dot{m}_p} = \frac{F}{\dot{m}} = \frac{I_b}{m} = b_{exp} K \qquad (16)$$

shows an average value $[w_e]_{div} \sim 12000$ m/s in diverging-anode thrusters and $[w_e]_{cyl} \sim 9800$ m/s. Considering an electromagnetic acceleration, this effective velocity finds its upper limit in the theoretical value

$$w_{th} = bK; \qquad (17)$$

which in the two cases respectively equals $[w_{th}]_{div} \approx 13300$ m/s and $[w_{th}]_{cyl} \approx 11500$ m/s. Anyway, the theoretical effective velocity is much lower than the measured one which, as already pointed out, is equal in both cases. All that proves that the discharge accelerates by Lorentz forces a much smaller mass (m_{acc}) than the ablated one (m); indeed, assuming that the non accelerated mass ($m_l = m - m_{acc}$) has null velocity,

$$w = \frac{I_b}{m_{acc}}\,; \qquad (18)$$

hence

$$\mu = \frac{m_{acc}}{m} = \frac{w_e}{w}\,, \qquad (19)$$

being respectively $\mu_{div} = 0.65$ and $\mu_{cyl} = 0.53$. According to these considerations, a higher specific impulse ($I_{sp} = F/\dot{m}g$) may be obtained by adopting smaller propellant effective surface areas (A_p).

In first approximation, the trends of the parameters obtained with varying E_0 in all thrusters further prove the "self-regulating" behaviour [equations (1) e (2)] typical of solid-propellant thrusters; this implies the same functioning, characterized by the same $K = I^2/\dot{m}$, in all regimes.

References

[1] Paccani G., *"Non-Steady Solid Propellant MPD Thruster Experimental Analysis Concepts"*, AIAA Paper 90-2674, AIAA/DGLR/JSASS 21st IEPC, Orlando, Florida, 18-20 July, 1990.

[2] Solbes A., Vondra R. J., *"Performance Study of a Solid Fuel-Pulsed Electric Microthruster"*, J. Spacecraft, vol. 10, n. 6, June 1973, pp. 406-410.

[3] Paccani G., Ravignani R., *"Sistema per la misura della spinta di propulsori MPD"*, XII Congresso Nazionale AIDAA, Como (I) 20-23 luglio, 1993.

[4] Paccani G., Di Zenzo S., *"MPD Thrusters Jet Time-of-flight Measurement by Cross-Correlation of Langmuir Double Probes Signals"*, forthcoming.

[5] Jahn R. G., *Physics of Electric Propulsion*, Mc Graw Hill Book Company, N.Y., 1968.

Acknowledgments

The author wishes to thank the student M. Di Gianvito who accurately carried out most of the measurements reported in this paper, in particular those concerning the segmented-anode thrusters, as well as the computer filing of all data.